J Mater Sci (2019) 54:4780–4787

Electronic materials

Highly conductive two-dimensional electron gas at the interface of $Al_2O_3/SrTiO_3$

Zhaoting Zhang[1], Hong Yan[1], Shuanhu Wang[1], Min Wang[1], Lixia Ren[1], Changle Chen[1], and Kexin Jin[1,*]

[1] *Shaanxi Key Laboratory of Condensed Matter Structures and Properties, School of Natural and Applied Sciences, Northwestern Polytechnical University, Xi'an 710072, China*

Received: 4 September 2018
Accepted: 20 November 2018
Published online: 26 November 2018

© Springer Science+Business Media, LLC, part of Springer Nature 2018

ABSTRACT

We create a two-dimensional electron gas at the $Al_2O_3/SrTiO_3/LaAlO_3$ heterostructures using pulsed laser deposition, which exhibits a decreasing sheet resistance with increasing growth temperatures of Al_2O_3 films. Structural characterizations of films are confirmed by cross-sectional transmission electron microscopy. Compared with these heterostructures with Al_2O_3 films deposited on pristine $SrTiO_3$ and TiO_2-terminated $SrTiO_3$ substrates, the $Al_2O_3/SrTiO_3/LaAlO_3$ heterostructures are more conductive. X-ray photoelectron spectroscopy indicates the formation of oxygen vacancies at the $SrTiO_3$ side of the interface, which results from the redox reactions by reducing $SrTiO_3$ films. Furthermore, the existence of oxygen vacancies on the $SrTiO_3$ side is verified by a blue-light emission.

Introduction

The discovery of two-dimensional electron gas (2-DEG) at the epitaxial heterointerfaces between two insulating perovskite oxides [1] provides potential opportunities for oxide-based electronic devices due to the intriguing properties, such as high electron mobility [2], superconductivity [3], magnetism [4–7], Rashba spin–orbital coupling [8]. At present, some dominant mechanisms have been proposed to explain the interfacial conductivity, including electronic reconstruction based on the polarization catastrophe, thermal interdiffusion of cation across the interface, strain-induced polarization and the creation of oxygen vacancies in $SrTiO_3$ (STO) substrates [1, 2, 9, 10]. In particular, it has been also demonstrated that a 2-DEG could be formed by growing amorphous oxide layers on TiO_2-terminated STO substrates, such as $LaAlO_3$ (LAO), Al_2O_3 and $YAlO_3$, and the conductivity is attributed to the presence of interfacial oxygen vacancies [11, 12]. In addition, 2-DEG at the interface between a spinel Al_2O_3 epitaxial films and STO substrates has been observed with an extremely high carrier mobility at 2 K [2]. Generally, the conductivity of 2-DEG at the heterointerfaces between Al_2O_3 films and STO can be dominated by many factors, such as substrate temperature, oxygen partial pressure and target–substrate distance [13]. In addition, different deposition methods, such as pulsed laser deposition (PLD),

Address correspondence to E-mail: jinkx@nwpu.edu.cn

https://doi.org/10.1007/s10853-018-3167-6

molecular beam epitaxy and atomic layer deposition, can also greatly influence the conductivity [14, 15]. In fact, one important role in the formation of a 2-DEG is single-crystalline TiO_2-terminated STO substrates used in growing functional oxides. This limits the realization of full potential of oxide 2-DEG devices in the technology integrating with semiconductors. One practicable way is to deposit a buffered STO layer, which offers the potential for overcoming the hurdles. Meanwhile, the high-mobility 2-DEGs at complex oxide interfaces not only show promise for multifunctional all-oxide devices with probably even richer behavior than that in bulk, but also would provide a wealth of opportunities to study mesoscopic physics with strongly correlated electrons confined in nanostructures. More importantly, this also contributes to the deep understanding of intrinsic mechanisms at interface conduction, such as the oxygen vacancies and the polar discontinuity. For this, we present a 2-DEG at interfaces between amorphous Al_2O_3 and buffered STO films pre-deposited on (100)-oriented LAO single-crystal substrates (Al_2O_3/STO/LAO). As a comparison, Al_2O_3 films are also deposited on pristine STO (Al_2O_3/P-STO) and TiO_2-terminated STO substrates (Al_2O_3/TiO_2-STO). The Al_2O_3/STO/LAO heterostructure with a Al_2O_3 film grown at 500 °C is more conductive with the electron Hall mobility as high as $\sim$ 164 $cm^2\ V^{-1}\ s^{-1}$ and the sheet carrier density of $\sim 10^{14}\ cm^{-2}$ at 20 K, which is similar to previous reports on LAO/STO [16]. The formation of 2-DEG can be attributed to oxygen vacancies at the interface created during the growth of Al_2O_3 films.

Experimental section

Commercially available $5 \times 5 \times 0.5\ mm^3$ stoichiometric LAO and STO single crystals with the (100) orientation were used in the present study. TiO_2-terminated STO surface was etched in buffered HF solution and followed by cleaning in deionized water and alcohol for 20 min. And then the substrate was annealed at 780 °C for 2 h to get a defect-free surface described previously [17]. Thin films of STO and Al_2O_3 sequentially were deposited on LAO single-crystal substrates by PLD using a KrF excimer laser (Lambda Physik, λ = 248 nm) with a laser fluence of 1.5 J cm^{-2} and the repetition rate of 1 Hz and 5 Hz, respectively. The epitaxial films of STO were deposited at 830 °C in an oxygen partial pressure of 1 Pa and then annealed for 30 min in situ. The Al_2O_3 films were deposited at 400, 500 and 600 °C (growth temperature, T_g) for 2 min at 6×10^{-4} Pa without the annealing treatment. The films were cooled down to room temperature at a rate of 5 °C/min under the deposition oxygen pressure. The thickness of STO and Al_2O_3 films was estimated by X-ray reflection (XRR) measurements by a PANalytical X'Pert Pro 95 X-ray diffractometer with Cu Kα X-ray source. Structural characterization was performed by high-resolution transmission electron microscopy (HRTEM, Tecnai G2 F20 S-TWIN) to confirm the epitaxial growth of films on LAO substrates. The surface morphology was investigated by atomic force microscopy (AFM, MFP-3D). Chemical composition and valence were analyzed by X-ray photoelectron spectroscopy measured with a photon energy of $h\nu$ = 1486.6 eV (XPS, Kratos Axis Ultra DLD). The photoluminescence (PL) spectrum of films was performed with a monochromatic light source consisting of a 150 W xenon lamp. Electrical measurements were carried out in a closed-cycle He refrigerator with quartz glass windows in the temperature ranging from 300 to 15 K. Hall effect of all heterostructures was measured in the Van der Pauw geometry, and the sheet resistance was measured in the standard four-probe geometry with ultrasonically wire-bonded aluminum wires as electrodes. Ohmic contact property was confirmed by linear current–voltage (*I*–*V*) characteristics.

Results and discussion

The structure of Al_2O_3/STO/LAO heterostructures is shown in Fig. 1a. The heterostructures are fabricated by depositing Al_2O_3 films on (100)-oriented LAO single-crystal substrates with a buffered STO layer. By the XRR measurements, the thicknesses of STO and Al_2O_3 films are estimated to be about 145 nm and 8 nm, respectively. As illustrated in Fig. 1b, the heterostructure grown at 500 °C shows an atomically flat granular surface with a *RMS* value of less than 600 pm, indicating high-quality films. To further characterize the samples, the cross-sectional TEM of Al_2O_3/STO/LAO heterostructure grown at 400 °C is examined. Figure 1c shows an abrupt interface from a crystalline state of STO films to an amorphous state, suggesting the amorphous growth of Al_2O_3 films at

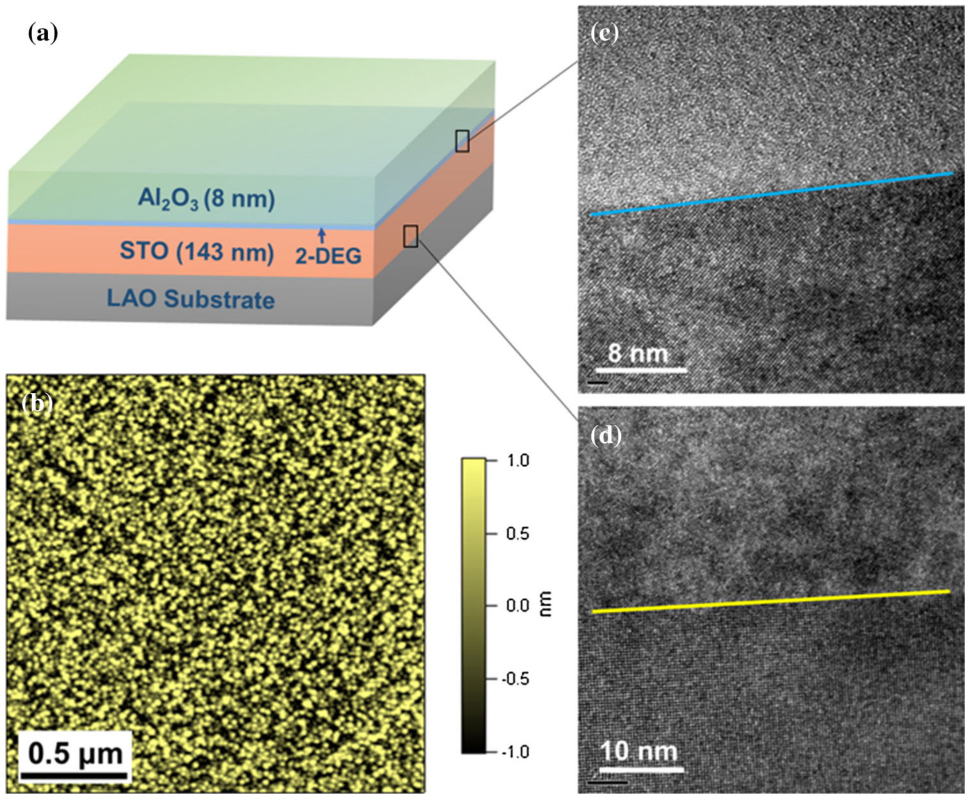

Figure 1 **a** Schematic figure of the heterostructure. **b** A representative surface morphology of the Al_2O_3/STO/LAO heterostructures with Al_2O_3 films grown at 500 °C. **c**, **d** The cross-sectional TEM images of the Al_2O_3/STO/LAO heterostructures with Al_2O_3 films grown at 400 °C.

400 °C. As shown in Fig. 1d, the results confirm the high degree of crystallinity of epitaxial STO films, providing an atomically smooth platform for the uniform growth of Al_2O_3 films.

Compared with the insulating STO/LAO interface deposited at the same conditions, the conductivity of Al_2O_3/STO/LAO heterostructures originates from the formation of 2-DEG at the interface between Al_2O_3 and STO films. The temperature dependence of sheet resistance for Al_2O_3/STO/LAO heterostructures at different T_g is shown in Fig. 2a. All samples show a metallic behavior and the metallicity becomes robust with increasing T_g. Namely, the room-temperature sheet resistance decreases with increasing growth temperatures of Al_2O_3 films. Interestingly, it is found that the metallic behavior of Al_2O_3/STO/LAO heterostructures shows a resistance minimum followed by an increase at low temperature, which is very different from the metallic behavior of pure 2-DEG [18]. The resistance upturn, which also has been observed at the amorphous LAO/STO interface [19], can be attributed to Kondo-like scattering between the interaction of charge carrier by localized spins associated with Ti^{3+} ions and the itinerant 2-DEG. Therefore, the resistance–temperature curves over the entire range are expressed on the basis of the following generalized equation [20]:

$$R = R_0 + R_a T^2 + R_b T^5 + R_K(T/T_K) \tag{1}$$

$$R_K(T/T_K) = R_{K,0}\left(\frac{1}{1 + (2^{1/s} - 1)(T/T_K)^2}\right)^s \tag{2}$$

where R_0 is the residual resistance due to the frozen-in disorder, the T^2 term comes from the electron–electron scattering and the T^5 contribution has its origin in the electron–phonon scattering. The last term is the Kondo contribution. $R_{K,0}$ is the Kondo resistance at zero temperature, and T_K is the Kondo temperature. The parameter s is fixed at 0.225 according to the theoretical result obtained from the numerical renormalization group. From the fits as shown in Fig. 2a, it is clear that Eq. (1) expresses the temperature dependence of resistance well. The fitting parameters are listed in Table 1. The fitted T_K values are 45.5, 96.2 and 88.1 K for the samples at T_g= 400, 500 and 600 °C, respectively. And they agree well with the experimental results in Fig. 2a. Therefore, the resistance upturn phenomenon observed in Al_2O_3/STO/LAO heterostructures can be attributed to Kondo scattering.

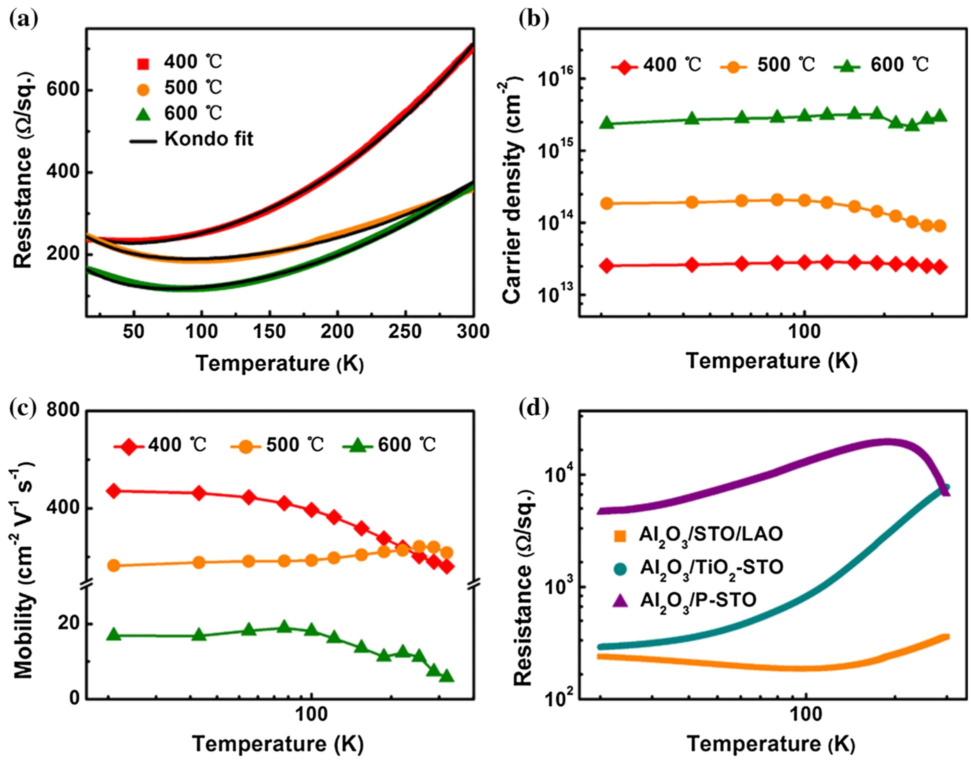

Figure 2 **a–c** Temperature dependence of sheet resistance, carrier density and electron Hall mobility for the interface at different growth temperatures of Al_2O_3 films. **d** Temperature dependence of sheet resistance for Al_2O_3/P-STO, Al_2O_3/TiO_2-STO and Al_2O_3/STO/LAO heterostructures.

The temperature-dependent sheet carrier density and mobility of Al_2O_3/STO/LAO heterostructures are illustrated in Fig. 2b, c. The negative Hall coefficient obtained by Hall-effect measurements favors electron-type charge carriers. The sheet carrier density is nearly constant in the whole temperature range for all Al_2O_3/STO/LAO heterostructures. With increasing Al_2O_3 growth temperature, the carrier density is enhanced by more than two orders of magnitude from 2.4×10^{13} to 3.0×10^{15} cm^{-2} at room temperature, while the corresponding Hall electron mobility decreases from 161.8 to 5.8 cm^{-2} V^{-1} s^{-1}. The very high carrier density for the sample grown in 600 °C may result in a 3D conductivity. These phenomena can be ascribed to oxygen vacancies which would be more at higher T_g [21]. Carrier density and Hall electron mobility of Al_2O_3/STO/LAO heterostructures are comparable with those of crystalline LAO/STO heterostructures [22]. The interface of Al_2O_3/$SrTiO_3$ on $LaAlO_3$ substrates presents a robust 2-DEG, which has a higher mobility than these integrated with non-STO substrates, such as the LAO/STO grown on Si substrates with ~ 10 cm^2 V^{-1} s^{-1} even at low temperatures [23]. It is noted that the increase of carrier density and the decrease of carrier mobility with increasing T_g lead to a decrease in the sheet resistance and further modulate the transport properties of 2-DEG. Moreover, the temperature-dependent carrier density and mobility of our Al_2O_3/STO/LAO heterostructures are similar to those of crystalline Al_2O_3/STO heterostructures [24]. Generally, dielectric constant (ε_r) of the STO increases with lowering temperature [25, 26]. As the ε_r increases, the dielectric screening of ionized scattering potentials should be boosted due to suppressed Coulomb potentials and consequently results in the detrapping of localized carriers. Hence, the electron–electron scattering will be enhanced with increasing carrier density, thus accounting for the decrease of mobility. For comparison, the Al_2O_3

Table 1 Fitting parameters of the R versus T data at Al_2O_3/STO/LAO heterostructures by using Eq. (1) over the entire temperature range

Sample (T_g/°C)	R_0 (Ω)	R_a (Ω/K^2)	R_b (Ω/K^5)	$R_{K,0}$ (Ω)	T_K (K)
400	333.346	0.01263	2.754×10^{-11}	288.047	45.515
500	77.700	0.00233	1.455×10^{-11}	181.639	96.244
600	4.621	0.00323	1.253×10^{-11}	176.936	88.134

films are deposited on TiO_2-terminated and pristine STO substrates at the growth temperature of 500 °C. The representative transport properties of heterostructures are shown in Fig. 2d. The Al_2O_3/TiO_2-STO heterostructure exhibits a metallic conduction, whereas the Al_2O_3/P-STO heterostructure becomes also conductive and favors a semiconductive behavior with a metal–insulator transition at 189.6 K. This phenomenon suggests TiO_2-terminated surface is not necessary for the creation of 2-DEG. In contrast, the Al_2O_3/STO/LAO heterostructure is much more conductive. Obviously, besides previously reported strong effect of thickness and target–substrate distance on the interface conduction, sheet resistance is also strongly dependent on the surface environment of substrate. Pristine STO surface has many microdefects due to the cutting and polishing during the preparation of STO. For the case of TiO_2-terminated STO substrate, etching the substrate in buffered HF solution effectively removes the surface defects and generates an atomic-scale smooth surface with regular terraces. In addition, oxygen vacancies are more easily created in the TiO_2-terminated STO surface, as the defect formation energy of TiO_2-terminated STO surface (5.94 eV) is considerably smaller than that of the bulk (7.17 eV) [27].

To verify the chemical nature and element composition of Al_2O_3/STO/LAO heterostructures, the XPS spectra of films are performed, showing clear signatures of the expected aluminum (Al), titanium (Ti) and oxygen (O) core levels with no detectable contamination. Normalized core levels spectra of Ti 2*p* for the surface of Al_2O_3/STO/LAO with T_g = 500 °C and STO/LAO heterostructures are shown in Fig. 3a. Normalized Ti 2*p* spectra of Al_2O_3/STO/LAO heterostructures show stronger Ti^{3+} signal than those of STO/LAO heterostructures, which indicates the generation of more oxygen vacancies in STO during the growth of Al_2O_3 layer by PLD [28]. Indeed, each oxygen vacancy releases two electrons that can occupy the initially empty Ti 3*d* band states, resulting in Ti^{3+} or even Ti^{2+} low-binding energy components. In Fig. 3b, the Ti $2p_{3/2}$ peaks for the Al_2O_3/STO/LAO heterostructures at different grown temperatures show a shoulder toward lower binding energy. It can be attributed to the emission from the 2*p* level of Ti^{3+}, which represents some additional electrons accumulated in the other empty 3*d* shell of Ti^{4+} in STO [29]. The presence of Ti^{3+} is probably a manifestation of the formation of oxygen vacancies at the STO side. The oxygen vacancies and the interfacial conductivity may result from the redox reactions at the interface by reducing STO films to oxidize the oxygen-deficient overlayer. It is noteworthy that a significant increase of the amount of Ti^{3+} is presented with increasing growth temperature from 400 to 600 °C, which strongly suggests an enhanced reduction of STO films and more oxygen vacancies [12]. This result strongly supports the fact that the two-dimensional conduction character results from interface-stabilized oxygen vacancies, confirming the changes of sheet resistance for the sample grown from 400 to 600 °C.

Figure 4 displays the room-temperature PL spectra of the Al_2O_3/STO/LAO heterostructures. All the samples show a broad luminescence band around 335–520 nm. The luminescence bands are distinctly asymmetrical in the spectral shape and consist of two broad visible emissions centered at around 365 nm (3.4 eV) and 390 nm (3.2 eV), which are close to the indirect gap energy (3.27 eV) and the direct gap energy (3.46 eV) of STO, respectively [30]. And the peak position with lower wavelength is slightly changed with the growth temperature of Al_2O_3 films, which is attributed to the variation of bandgap. These results manifest that STO films dominate the PL spectra in Al_2O_3/STO/LAO system. The long tail of PL spectra between around 400 and 520 nm shows a blue-light emission. This suggests that oxygen vacancies on the STO side may be the origin of blue-light emission, which agrees with the case of electron-doped STO and LAO/STO heterointerfaces [18, 31]. The luminescence intensity of Al_2O_3/STO/LAO is significantly increased with increasing growth temperatures of Al_2O_3 films. This behavior is consistent with the sheet resistance, implying that the luminescence has a close relationship with the metallic conduction caused by the oxygen vacancy. These oxygen vacancies can form the defect levels in the bandgap and may be responsible for the luminescence emission [18]. The increase of PL intensity can be attributed to the increasing oxygen vacancies in accordance with the conductivity with increasing growth temperatures. In other words, these results suggest that the interfacial conductivity of Al_2O_3/STO/LAO originates from oxygen vacancies at the STO side.

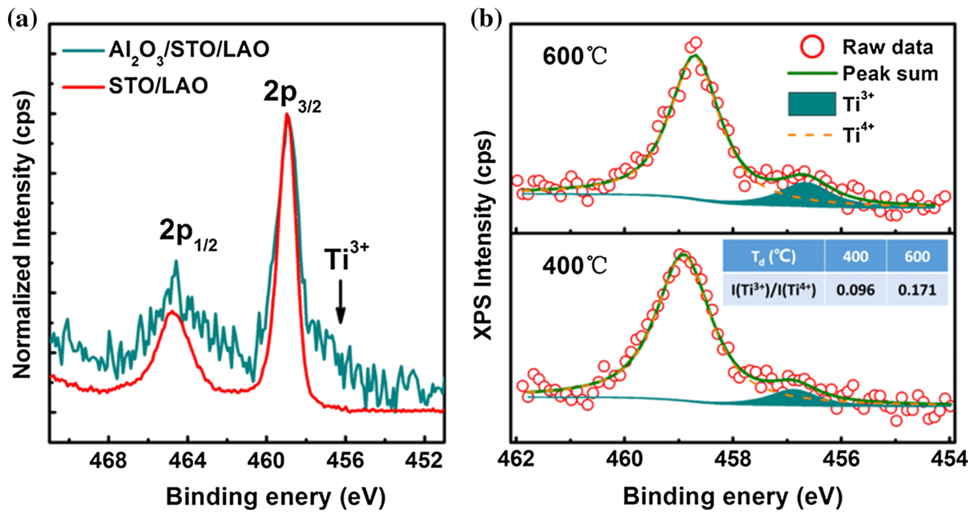

T_d (°C)	400	600
$I(Ti^{3+})/I(Ti^{4+})$	0.096	0.171

Figure 3 **a** Ti 2*p* XPS spectra for the STO/LAO and Al_2O_3/STO/LAO heterostructures. **b** Ti $2p_{3/2}$ XPS spectra for the Al_2O_3/STO/LAO heterostructures with Al_2O_3 films grown at different temperatures.

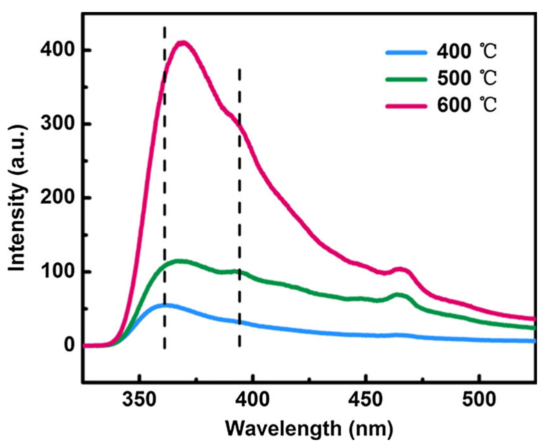

Figure 4 Room-temperature PL characteristics of Al_2O_3/STO/LAO heterostructures with Al_2O_3 films grown at different temperatures.

Summary and conclusions

In summary, we have obtained a 2-DEG at the Al_2O_3/STO/LAO heterostructures using pulsed laser deposition. And the conductivity is closely related to the growth temperature and dominated by oxygen vacancies at the STO side of interface. In addition, the Al_2O_3/STO/LAO heterostructures are more conductive than Al_2O_3/P-STO and Al_2O_3/TiO_2-STO heterostructures. X-ray photoelectron spectroscopy of the Ti 2*p* core level indicates the formation of oxygen vacancies at the STO side of interface. The PL spectra demonstrate that oxygen vacancies dominate the interfacial conductivity of Al_2O_3/STO/LAO heterostructures. These results promote the generation of oxide electronic devices and contribute to further understand the origin of 2-DEG at oxide interfaces.

Acknowledgements

This work is supported by the National Natural Science Foundation of China (Nos. 51572222, 51172183 and 61471301).

Compliance with ethical standards

Conflict of interest The authors declare no competing financial interest.

References

[1] Ohtomo A, Hwang HY (2004) A high-mobility electron gas at the $LaAlO_3$/$SrTiO_3$ heterointerface. Nature 427:423–426

[2] Chen YZ, Bovet N, Trier F, Christensen DV, Qu FM, Andersen NH, Kasama T, Zhang W, Giraud R, Dufouleur J, Jespersen TS, Sun JR, Smith A, Nygård J, Lu L, Büchner B, Shen BG, Linderoth S, Pryds N (2013) A high-mobility two-dimensional electron gas at the spinel/perovskite interface of γ-Al_2O_3/$SrTiO_3$. Nat Commun 4:1371

[3] Reyren N, Thiel S, Caviglia AD, Kourkoutis LF, Hammerl G, Richter C, Schneider CW, Kopp T, Rüetschi AS, Jaccard D, Gabay M, Muller DA, Triscone JM, Mannhart J (2007) Superconducting interfaces between insulating oxides. Science 317:1196–1199

[4] Brinkman A, Huijben M, van Zalk M, Huijben J, Zeitler U, Maan JC, van der Wiel WG, Rijnders G, Blank DHA, Hilgenkamp H (2007) Magnetic effects at the interface between non-magnetic oxides. Nat Mater 6:493–496

[5] Ariando Wang X, Baskaran G, Liu ZQ, Huijben J, Yi JB, Annadi A, Barman AR, Rusydi A, Dhar S, Feng YP, Ding HHJ, Venkatesan T (2011) Electronic phase separation at the $LaAlO_3/SrTiO_3$ interface. Nat Commun 2:188

[6] Li L, Richter C, Mannhart J, Ashoori RC (2011) Coexistence of magnetic order and two-dimensional superconductivity at $LaAlO_3/SrTiO_3$ interfaces. Nat Phys 7:762–766

[7] Bert JA, Kalisky B, Bell C, Kim M, Hikita Y, Hwang HY, Moler KA (2011) Direct imaging of the coexistence of ferromagnetism and superconductivity at the $LaAlO_3/SrTiO_3$ interface. Nat Phys 7:767–771

[8] Caviglia AD, Gabay M, Gariglio S, Reyren N, Cancellieri C, Triscone JM (2010) Tunable Rashba spin-orbit interaction at oxide interfaces. Phys Rev Lett 104:126803

[9] Chen YZ, Trier F, Kasama T, Christensen DV, Bovet N, Balogh ZI, Li H, Thydén KTS, Zhang W, Yazdi S, Norby P, Pryds N, Linderoth S (2015) Creation of high mobility two-dimensional electron gases via strain induced polarization at an otherwise nonpolar complex oxide interface. Nano Lett 15:1849–1854

[10] Chambers SA, Engelhard MH, Shutthanandan V, Zhu Z, Droubay TC, Qiao L, Sushko PV, Feng T, Lee HD, Gustafsson T, Garfunkel E, Shah AB, Zuo JM, Ramasse QM (2010) Instability, intermixing and electronic structure at the epitaxial $LaAlO_3/SrTiO_3$(001) heterojunction. Surf Sci Rep 65:317–352

[11] Lee SW, Liu YQ, Heo J, Gordon RG (2012) Creation and control of two-dimensional electron gas using Al-based amorphous oxides/$SrTiO_3$ heterostructures grown by atomic layer deposition. Nano Lett 12:4775–4783

[12] Chen YZ, Pryds N, Kleibeuker JE, Koster G, Sun JR, Stamate E, Shen BG, Rijnders G, Linderoth S (2011) Metallic and insulating interfaces of amorphous $SrTiO_3$-based oxide heterostructures. Nano Lett 11:3774–3778

[13] Chen YZ, Bovet N, Kasama T, Gao WW, Yazdi S, Ma C, Pryds N, Linderoth S (2014) Room temperature formation of high-mobility two-dimensional electron gases at crystalline complex oxide interfaces. Adv Mater 26:1462

[14] Kormondy KJ, Posadas AB, Ngo TQ, Lu SR, Goble N, Sweet JJ, Gao XPA, Smith DJ, McCartney MR, Ekerdt JG, Demkov AA (2015) Quasi-two-dimensional electron gas at the epitaxial alumina/$SrTiO_3$ interface: control of oxygen vacancies. J Appl Phys 117:095303

[15] Ngo TQ, Goble NJ, Posadas A, Kormondy KJ, Lu SR, McDaniel MD, Sweet JJ, Smith DJ, Gao XPA, Demkov AA, Ekerdt JG (2015) Quasi-two-dimensional electron gas at the interface of γ-$Al_2O_3/SrTiO_3$ heterostructures grown by atomic layer deposition. J Appl Phys 118:115303

[16] Rizi MY, Marsik P, Mallett BPP, Dubroka A, Christensen DV, Chen YZ, Pryds N, Bernhard C (2016) Infrared ellipsometry study of the confined electrons in a high-mobility γ-$Al_2O_3/SrTiO_3$ heterostructure. Europhys Lett 113:47005

[17] Yan H, Zhang ZT, Wang SH, Wei XY, Chen CL, Jin KX (2018) Magnetism control by doping in $LaAlO_3/SrTiO_3$ heterointerfaces. ACS Appl Mater Interfaces 10:14209–14213

[18] Kalabukhov A, Gunnarsson R, Börjesson J, Olsson E, Claeson T, Winkler D (2007) Effect of oxygen vacancies in the $SrTiO_3$ substrate on the electrical properties of the $LaAlO_3/SrTiO_3$ interface. Phys Rev B 75:121404

[19] Liu GZ, Qiu J, Jiang YC, Zhao R, Yao JL, Zhao M, Feng Y, Gao J (2016) Light induced suppression of Kondo effect at amorphous $LaAlO_3/SrTiO_3$ interface. Appl Phys Lett 109:031110

[20] Yan H, Zhang ZT, Wang SH, Zhang HR, Chen CL, Jin KX (2017) Modulated transport behavior of two-dimensional electron gas at Ni-doped $LaAlO_3/SrTiO_3$ heterointerfaces. ACS Appl Mater Interfaces 9:39011–39017

[21] Rastogi A, Pulikkotil JJ, Auluck S, Hossain Z, Budhani RC (2012) Photoconducting state and its perturbation by electrostatic fields in oxide-based two-dimensional electron gas. Phys Rev B 86:075127

[22] Mannhart J, Schlom DG (2010) Oxide interfaces: an opportunity for electronics. Science 327:1607–1611

[23] Park JW, Bogorin DF, Cen C, Felker DA, Zhang Y, Nelson CT, Bark CW, Folkman CM, Pan XQ, Rzchowski MS, Levy J, Eom CB (2010) Creation of a two-dimensional electron gas at an oxide interface on silicon. Nat Commun 1:94

[24] Niu W, Gan YL, Zhang Y, Christensen DV, von Soosten M, Wang XF, Xu YB, Zhang R, Pryds NN, Chen YZ (2017) Suppressed carrier density for the patterned high mobility two-dimensional electron gas at γ-$Al_2O_3/SrTiO_3$ heterointerface. Appl Phys Lett 111:021602

[25] Lippmaa M, Nakagawa N, Kawasaki M (2000) Dielectric properties of homoepitaxial $SrTiO_3$ thin films grown in the step-flow mode. J Electroceram 4:365

[26] Sakudo T, Unoki H (1971) Dielectric properties of $SrTiO_3$ at low temperatures. Phys Rev Lett 26:851–853

[27] Carrasco J, Illas F, Lopez N, Kotomin EA, Zhukovskii YF, Evarestov RA, Mastrikov YA, Piskunov S, Maier J (2006) First principles calculations of the atomic and electronic structure of F centers in the bulk and on the (001) surface of $SrTiO_3$. Phys Rev B 73:064106

[28] Lee SW, Heob J, Gordon RG (2013) Origin of the self-limited electron densities at $Al_2O_3/SrTiO_3$ heterostructures grown by atomic layer deposition–oxygen diffusion model. Nanoscale 5:8940–8944

[29] Sing M, Berner G, Goß K, Müller A, Ruff A, Wetscherek A, Thiel S, Mannhart J, Pauli SA, Schneider CW, Willmott PR,

Gorgoi M, Schäfers F, Claessen R (2009) Profiling the interface electron gas of $LaAlO_3/SrTiO_3$ heterostructures with hard X-ray photoelectron spectroscopy. Phys Rev Lett 102:176805

[30] Mochizuki S, Fujishiro F, Minami S (2005) Photoluminescence and reversible photo-induced spectral change of $SrTiO_3$. J Phys Condens Matter 17:923–948

[31] Kan D, Terashima T, Kanda R, Masuno A, Tanaka K, Chu S, Kan H, Ishizumi A, Kanemitsu Y, Shimakawa Y, Takano M (2005) Blue-light emission at room temperature from Ar^+-irradiated $SrTiO_3$. Nat Mater 4:816–819